Metrol. Meas. Syst., Vol. 31 (2024), No. 4
DOI: 10.24425/mms.2024.152051

METROLOGY AND MEASUREMENT SYSTEMS
Index 330930, ISSN 0860-8229
www.metrology.wat.edu.pl

H∞ CONTROL AND EXPERIMENTAL STUDY OF MR SEMI-ACTIVE SUSPENSION WITH ACTUATOR RESPONSE DELAY

Renkai Ding[1)], Ping Wang[2)], Anze Li[3)], Ruochen Wang[4)], Dong Sun[4)], Ke Xu[5)]

1) *State Key Laboratory of Automotive Simulation and Control, Jilin University, Changchun, Jilin 130015, China*, (*drk@ujs.edu.cn*)
2) *School of Communication Engineering, Jilin University, Changchun, Jilin 130015, China*
3) *Automotive Engineering Research Institute, Jiangsu University, Zhenjiang 212013, China*
4) *School of Automotive and Traffic Engineering, Jiangsu University, Zhenjiang 212013, China*
5) *Jiangsu Tangchen Automotive Parts Co., Ltd;*

Abstract

Given the potential negative impact of delayed response from magnetorheological (MR) damper on the effectiveness of semi-active suspension (SAS), a specialized time-delay dependent H_∞ robust controller has been developed to address this issue. The controller accounts for the actuator response delay, and determines the system theoretical critical delay. To mitigate the response delay within the electromagnetic loop of the actuator, a technique has been proposed and tested. The technique aims to minimize the overall response delay, ensuring it is less than the theoretical critical delay. Subsequently, feedback gain is determined and comparative performance tests are conducted to validate the efficacy of the proposed control method. Comparing with a delay-independent H_∞ robust controller, it has been demonstrated that the body acceleration and dynamic tire load peak-to-peak responses generated by proposed controller are decreased by 16.4% and 7.4% respectively under bumpy road conditions, while under stochastic road conditions, body acceleration decreases by 3.5%, suspension deflection by 17.1%, and DTL by 0.89%.

Keywords: Semi-active suspension, Actuator response delay, Time-delay dependent H_∞ robust controller, Theoretical critical delay, Comparative performance test.

1. Introduction

The magnetorheological *semi-active suspension* (SAS) dynamically adapts damping based on prevailing driving conditions, combining the universality and adaptability of active suspension [1-3] with low energy consumption. This has garnered significant attention and application [4]. However, time delay can have a negative impact on control effectiveness. If the controller design overlooks the issue of delay, it may result in inconsistent output from the controller and input to the MR damper, rendering the feedback loop ineffective and degrading control performance. Furthermore, instability in the controlled object itself can lead to system instability. Although some literature [5] suggests that semi-active systems naturally exhibit stability and that issues related to time delay causing instability are unlikely, this viewpoint lacks rigor.

The delay of magnetorheological SAS is mainly comprised of four aspects, as proposed in the literature [6]. The control force phase will demonstrate a specific overall time delay, encompassing the individual time delays of each component. Effectively managing the time delay of other components becomes challenging once the controller or actuator is designed, with the exception of the actuator response delay. Therefore, the primary focus in investigating time delays in SAS systems revolves around addressing response delays. Currently, there are two approaches to address the system response delay. One approach is Smith predictive control [7-9], while the other involves robust control based on Lyapunov-Krasovskii stability theory

Article history: received May 15, 2025; revised July 31, 2024; accepted August 12, 2023; available online October 15, 2024.

[10-12]. The Smith predictive controller relies on an accurate mathematical model. The presence of a model mismatch between the theoretical model and the actual device can result in poor closed-loop performance. The main idea of robust control based on Lyapunov-Krasovskii stability theory is to construct a Lyapunov-Krasovskii functional or Lyapunov function and ensure its stability. Li [13] Li developed a nonlinear system model that considers the time delay of the CDC system. The study focused on analyzing the impact of the time delay on vehicle performance. Yang [14] Yang conducted a multi-objective optimization design for a time-delay feedback dynamic vibration absorber system with inertial stiffness. Through the optimization of both the system structure parameters and control parameters, effective control over the formant amplitude, anti-formant amplitude, and anti-resonance band symmetry of the main system was achieved. Liu [15] proposed a comprehensive solution for analyzing the variation pattern of critical instability time-delay in *inerter-spring-damper* (ISD) suspension. Based on the analysis findings, a method for selecting suspension parameters that can reduce the impact of time delay is suggested. To improve the potential for energy harvesting and enhance the driving stability of nonlinear time-delay active suspension systems, Wu [16] introduced time-delay active control technology. Moreover, in order to validate the effectiveness of the proposed method, a bench test was conducted using the dSPACE system. Zhu [17] proposed a delay dependent sliding mode variable structure control method. To validate the actual performance, a real vehicle test was conducted. The conventional sliding mode controller and Smith compensation controller were used for comparison during the test. The results demonstrated that the proposed controller outperformed the other two controllers. In order to investigate the potential and impact of the optimal time-delay feedback control, Nan [18] conducted a comparative experiment using active suspension equipment provided by Canada's Quanser Company. The experimental results indicate that, in comparison to LQR control, the proposed control method resulted in a 39.18% reduction in sprung mass acceleration under harmonic excitation and a 35.5% reduction under random road excitation.

To guarantee the system stability, designing a state feedback controller with time delay dependence is necessary, and make sure the system stability by solving a given anti-jamming coefficient of critical delay, thus, the controller gain is obtained. However, the correlation between the theoretical critical delay and the actual response delay is often overlooked. Existing research frequently assumes that the response delay falls within the theoretical critical delay range, and then only verifies the rationality and effectiveness of the controller through simulation analysis. However, not all actuator response delays fall within the theoretical critical delay range. When the former exceeds the latter, it hinders effective controller gain acquisition. Additionally, different Lyapunov-Krasovskii generic functions will impact delay-dependent controller design. Even with identical anti-interference coefficients, different delay-dependent controllers will have varying theoretical critical delays. Consequently, for a given actuator, one must consider the relationship between actual response delay and the theoretical critical delay of the designed delay-dependent controller. Therefore, it is clear that existing assumptions are unreasonable.

The research is focused on the MR SAS system, with a specific emphasis on designing a time-delay dependent H∞ robust controller to address the actuator response delay. The theoretical critical delay is determined by specifying the anti-interference coefficient. Based on this, the actual actuator response delay is measured, and a method for reducing this delay is proposed to ensure that it falls within the theoretical critical time range. This in turn allows for obtaining the controller feedback gain.

The innovations outlined in this paper are as follows: the relationship between the actual response delay and the theoretical critical delay of the designed delay-dependent controller is considered. It is noted that existing researches usually assume that the actuator response delay falls within the theoretical critical delay range. Additionally, a method is put forward to

minimize the response delay of the electromagnetic loop of MR damper, thereby decreasing its overall response delay and ensuring that it remains less than the theoretical critical delay allowed by the controller.

2. MR SAS model

2.1. MR damper model

Considering that the Bingham model has advantages of simple structure, clear physical meaning of parameters and good engineering practicability. The Bingham mechanical model is expressed as [19]:

$$\begin{cases} F(t) = c_e v(t) + F_{MR}(t)\,\mathrm{sgn}(v(t)) \\ F_{MR}(t) = a_4 I^4(t) + a_3 I^3(t) + a_2 I^2(t) + a_1 I(t) + a_0 \end{cases} \tag{1}$$

Where, $F(t)$ represents the output control force; c_e represents viscous damping coefficient; $v(t)$ denotes the motion velocity; $F_{MR}(t)$ represents the coulomb damping force; sgn(·) represents a symbolic function; I represents the control current; a_i (i =0, 1, 2, 3, 4) is the constant to be fitted.

In actual, the controller calculates the control current based on the ideal control force in order to output the corresponding control force. Therefore, it is essential to use the current as the control quantity, establish a correlation between coulomb damping force and control current, and develop an inverse model. In this paper, the computing speed, fitting error and fitting effect of the system are considered comprehensively, and the relation is fitted as a first-order linear relation:

$$I(t) = b_1 F_{MR}(t) + b_0 \tag{2}$$

Where, b_0 and b_1 are constants to be fitted.

The maximum motion stroke is 90mm, and the maximum input current is 3.5 A. The indicator diagram and speed characteristic curve measured by INSTRON 8800 numerical control hydraulic servo vibration test bench (Fig. 1a) are shown in Fig. 1b. According to the test results, c_e=854.2 $N{\cdot}s/m$, a_0=2.03, a_1=59.24, a_2=421.8, a_3=-181.71, a_4=24.8, b_1=-0.008248, b_2=0.002574.

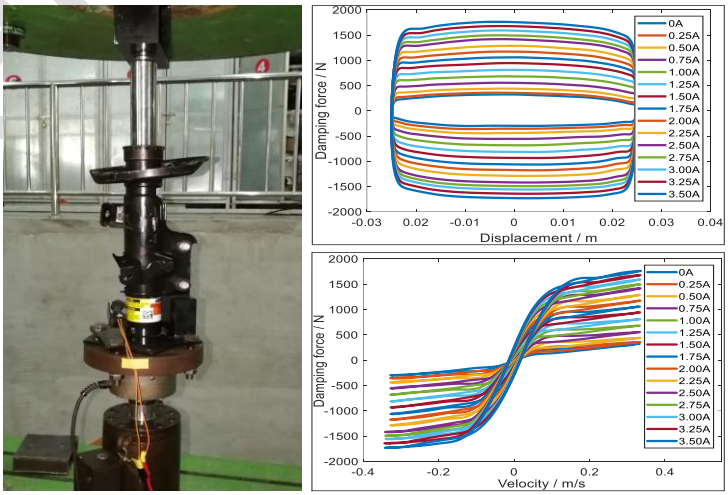

(a) Test bench (b) Test results
Fig. 1. Characteristic test.

2.2. Response delay model

A 1/4 SAS model (Fig. 1) is established, and the system dynamics is as follows:

$$\begin{cases} m_s\ddot{x}_s(t)+c_e(\dot{x}_s(t)-\dot{x}_u(t))+k_s(x_s(t)-x_u(t))=u(t-\tau) \\ m_u\ddot{x}_u(t)-c_e(\dot{x}_s(t)-\dot{x}_u(t))+c_t(\dot{x}_u(t)-\dot{x}_r(t))-k_s(x_s(t)-x_u(t))+k_t(x_u(t)-x_r(t))=-u(t-\tau). \end{cases} \tag{3}$$

And

$$u(t-\tau)=\begin{cases} F_{MR}(t-\tau)\,\mathrm{sgn}(v(t)) & if\ \ F_{MR}(t-\tau)\,\mathrm{sgn}(v(t))\cdot(v(t))<0 \\ 0 & if\ \ F_{MR}(t-\tau)\,\mathrm{sgn}(v(t))\cdot(v(t))\geq 0 \end{cases}, \tag{4}$$

where, m_s and m_u represent sprung mass and unsprung mass, respectively, k_s and k_t represent spring stiffness and tire stiffness, respectively, c_t represents tire damping coefficient, x_s symbolizes the sprung mass stroke, x_t symbolizes the mass stroke, x_r represents road excitation, $u(t-\tau)$ represents the control input with variable time delay, τ represents the actuator response delay.

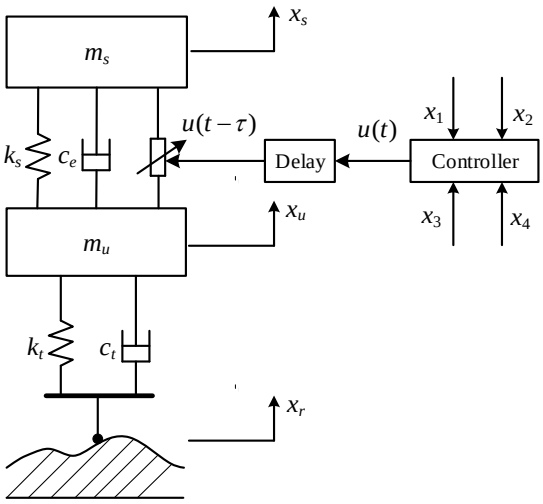

Fig. 2. MR SAS model.

Let $X(t)=\left[x_1(t), x_2(t), x_3(t), x_4(t)\right]^T$, $Y(t)=\left[y_1(t), y_2(t), y_3(t)\right]^T$, $Z(t)=\left[z_1(t), z_2(t), z_3(t), z_4(t)\right]^T$, $U(t-\tau)=u(t-\tau)$, $W=\dot{x}_r(t)$. And $x_1(t)=x_s(t)-x_u(t)$, $x_2(t)=x_u(t)-x_r(t)$, $x_3(t)=\dot{x}_s(t)$, $x_4(t)=\dot{x}_u(t)$, $y_1(t)=\ddot{x}_s(t)$, $y_2(t)=x_s(t)-x_u(t)$, $y_3(t)=x_u(t)-x_r(t)$, $z_1(t)=x_1(t)$, $z_2(t)=x_2(t)$, $z_3(t)=x_3(t)$, $z_4(t)=x_4(t)$, $\dot{x}_r(t)$ is road velocity input. And the system equation can be obtained:

$$\begin{cases} \dot{X}(t)=AX(t)+BU(t-\tau)+EW(t) \\ Y(t)=CX(t)+DU(t-\tau) \\ Z(t)=GX(t) \end{cases} \tag{5}$$

$$A=\begin{bmatrix} 0 & 0 & 1 & -1 \\ 0 & 0 & 0 & 1 \\ -k_s/m_s & 0 & -c_e/m_s & c_e/m_s \\ k_s/m_u & -k_t/m_u & c_e/m_u & -(c_e+c_t)/m_u \end{bmatrix}, \quad B=\begin{bmatrix} 0 \\ 0 \\ 1/m_s \\ -1/m_u \end{bmatrix}, \quad E=\begin{bmatrix} 0 \\ -1 \\ 0 \\ c_t/m_u \end{bmatrix},$$

$$C=\begin{bmatrix} -k_s/m_s & 0 & -c_e/m_s & c_e/m_s \\ 1 & 0 & 0 & 0 \\ 0 & 1 & 0 & 0 \end{bmatrix}, \quad D=\begin{bmatrix} 1/m_s \\ 0 \\ 0 \end{bmatrix},$$ G is the identity matrix.

The evaluation criteria are shown in (6) to (8), respectively [20].

$$\left\|A_{acc}\right\|_{rms}=\sqrt{\frac{1}{T}\int_0^T\left\|\ddot{x}_s\right\|^2 dt} \tag{6}$$

$$\left\|F_{dtl}\right\|_{rms}=k_t\sqrt{\frac{1}{T}\int_0^T\left\|x_u-x_r\right\|^2 dt} \tag{7}$$

$$\left\|f_{sws}\right\|_{rms}=\sqrt{\frac{1}{T}\int_0^T\left\|x_s-x_u\right\|^2 dt} \tag{8}$$

Where, $A_{acc\ \ rms}$ denotes the *root mean square* (RMS) of *body acceleration* (BA), which is commonly used to evaluate the ride comfort; $F_{dtt\ \ rms}$ denotes the RMS of the *dynamic tire load* (DTL), which is usually adopted to evaluate the handling performance; $f_{svs\ \ mms}$ denotes the RMS of the *suspension deflection* (SD), which is usually used as s system constraint to evaluate the vehicle safety; T is the length of the sampled data.

3. Delay-dependent H_∞ robust controller

In order to design a time-delay dependent H_∞ robust controller for SAS, it is necessary to develop a memoryless feedback control law based on (5) to meet the system performance criteria. The feedback control law can be expressed as follows:

$$U(t)=KX(t) \tag{9}$$

Where, K is the gain matrix of state feedback.

According to (5) and (9), the closed-loop system can be obtained:

$$\begin{cases} \dot{X}(t)=AX(t)+BKX(t)+EW(t) \\ Y(t)=CX(t)+DKX(t) \\ Z(t)=GX(t) \\ X(t)=\phi(t), \quad \forall t\in[-\tau,0] \end{cases} \tag{10}$$

Under the condition of finite energy input signal $W(t)\in L_2[0,\infty)$, the closed-loop system shall meet the subsequent design specification:

(1) The closed-loop system exhibits asymptotically stable;

(2) For the given anti-interference coefficient γ, in the case of zero initial value, it is required that the closed-loop system should be satisfied as $\left\|Y(t)\right\|_2<\gamma\left\|W(t)\right\|_2$.

In order to mitigate the impact of actuator response delay on system control effectiveness, a Lyapunov-Krasovskii function is constructed:

$$V(t)=V_1(t)+V_2(t)+V_3(t) \tag{11}$$

where,

$$V_1(t)=X^T(t)P_1X(t) \tag{12}$$

$$V_2(t)=\int_{-\tau}^{0}\int_{t+\beta}^{t}\dot{X}^T(\alpha)Z_2\dot{X}(\alpha)d\alpha d\beta \tag{13}$$

$$V_3(t)=\int_{t-\tau}^{0}\int_{t+\beta}^{t}\dot{X}^T(\alpha)Q_1\dot{X}(\alpha)d\alpha d\beta \tag{14}$$

The positive definite symmetric matrices P_1, Z_2 and Q_1 are the matrices to be solved, which are used to guarantee the negative definite of (11).

Assuming zero initial condition, that is for $\forall t\in[-\tau,0]$ and $\phi(t)=0$, there is $V(t)\big|_{t=0}=0$. Next, the H_∞ performance of the system will be analyzed, taking into consideration the following indicators:

$$J_{YW}=\int_0^\infty\left[Z^T(t)Z(t)-\gamma^2W^T(t)W(t)\right]dt \tag{15}$$

For all non-zero $W(t)\in L_2[0,\infty)$, if the negative definite of the Lyapunov-Krasovskii function (11) is guaranteed, we can further obtain:

$$\begin{aligned}J_{YW}&\le\int_0^\infty\left[Z^T(t)Z(t)-\gamma^2W^T(t)W(t)\right]dt+V(t)\big|_{t=\infty}-V(t)\big|_{t=0}\\&=\int_0^\infty\left[Z^T(t)Z(t)-\gamma^2W^T(t)W(t)+\dot{V}(t)\right]dt\\&=\int_0^\infty\eta^T(t)\Pi\eta(t)dt\end{aligned} \tag{16}$$

where,

$$\eta(t)=\left[X(t),\ X(t-\tau),\ W(t)\right]^T$$

$$\Pi=\begin{bmatrix}\Phi_1 & \Phi_2 & \tau A^TZ_2E+P_1E\\ \Phi_2^T & \Phi_3 & \tau K^TB^TZ_2E\\ \tau E^TZ_2A+E^TP_1 & \tau E^TZ_2BK & -\gamma^2I+\tau E^TZ_2E\end{bmatrix}$$

$$\Phi_1=A^TP_1+P_1A+\tau X_1+Y_1+Y_1^T+Q_1+\tau A^TZ_2A+C^TC$$

$$\Phi_2=P_1BK-Y_1+\tau A^TZ_2BK+C^TDK,\quad \Phi_3=-Q_1+\tau K^TB^TZ_2BK+K^TD^TDK.$$

Then the H_∞ performance $\|Y(t)\|_2<\gamma\|W(t)\|_2$ can be achieved. The (16) can be analyzed for its existence and stability conditions using the LMI method, while the critical delay of the system can be determined through conic complement linearization iteration. These methods enable the derivation and solution of key properties related to the equation and system in a rigorous and systematic manner. In this paper, a conical complement linearization iterative algorithm [21] is adopted to solve the problem, and the dichotomy method [22] on the basis of given anti-interference coefficient γ is used to solve critical delay τ_{max}.

Taking into account the limitations related to BA, SD, and DTL, as well as considering the functional relationship between the anti-interference coefficient and H_∞ robust performance in gaming, an anti-interference coefficient of γ=12.5 is chosen. The cone complement linearization iterative algorithm and dichotomy method are utilized to determine the critical delay τ_{max}=29.2 ms.

4. Response delay analysis

The approach to solving the gain of the delay-dependent H_∞ robust controller is to pre-set the system response delay and anti-interference coefficient. If the system is in a state of instability ($\tau_{act} > \tau_{max}$), it is not possible to obtain the feedback gain of the H_∞ delay-dependent robust controller [23]. To verify the feasibility of the proposed control method, this paper tests the true actuator response delay. Literature [23] introduces the concept of response delay for an MR damper, which is defined as the time required for the system to transition from one stable state to another, encompassing 63.2% of total transition time when there are changes in system state. Since determining the response delay of an MR damper involves considering interaction between both response time of electromagnetic loop and time required to establish control force, theoretical analysis alone cannot clearly distinguish specific stages at which these occur; therefore, overall response delay can only be determined through experimentation. To this end, an open-loop control system for an MR damper comprising components such as current driver, current sensor, oscilloscope, power supply and signal generator is first established as shown in Fig. 3a.

(a) Open-loop system. (b) Closed-loop system.

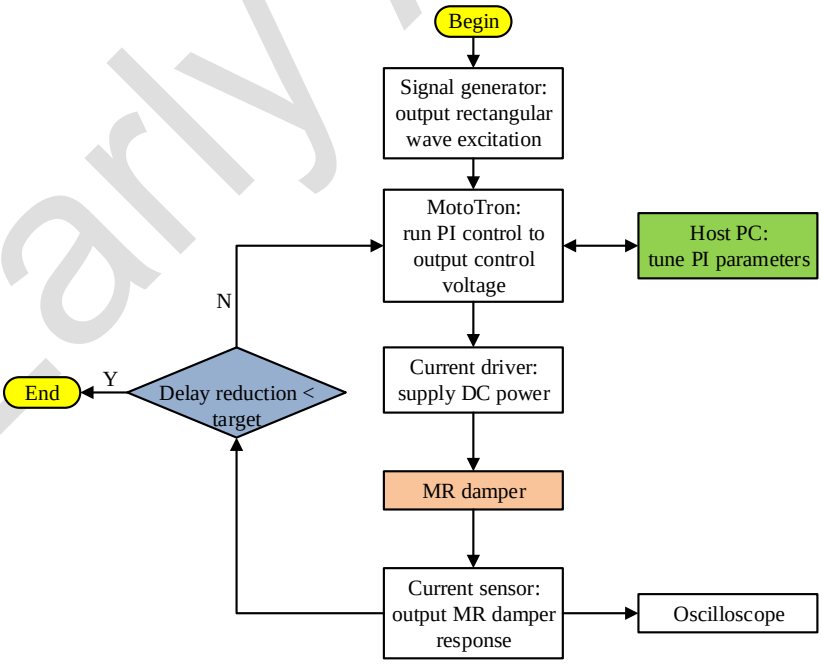

(c) Flow chat of the closed-loop control experiment.
Fig. 3. Control system of MR damper.

The purpose here is mainly focused on testing response time within electromagnetic loops related to an MR damper. Specifically, the current driver transmits separate current signals to

the MR damper, and the response is measured by the current sensor. The electromagnetic response time of different input currents is then calculated. The specific flow of the closed-loop control experiment is shown in Fig. 3c, and the test results are displayed within Fig. 4a. It is evident that the open-loop response time T_u of upper step (current loading) ranges from 40 to 50ms, while the open-loop response time T_d of the lower step (current cut-off) ranges from 38 to 43ms. It has been seen that as the input current increases, the response time decreases. However, both the load time and cut-off time exceed theoretical critical delay limits. When factoring in setup time needed for control force, it becomes clear that actual response delay will surpass system's allowed theoretical critical delay for maintaining stability.

A PI control method has been developed to minimize response delay, as shown in Fig. 3b. In comparison with the open-loop control system, both an upper computer and MotoTron system have been added. The specific test process is as follows: first, the sensor model, PI algorithm, and output model are constructed in the upper computer and then compiled and downloaded into the MotoTron system. Next, a signal generator outputs the test condition to the MotoTron system. The MotoTron system operates the PI algorithm and outputs a target control voltage (*i.e.*, PWM signal) to the current driver; subsequently, the driver inputs this target current to the MR damper. Feedback on actual current signal is provided by a series-connected current sensor in order to enable closed-loop PI control of driving current within circuit operation. The power supply is utilized to provide power to the MotoTron system and current drivers. The oscilloscope is used to display the real-time current response of the drive, while the upper computer is employed for recording data. The response characteristics using a PI control algorithm are depicted in Fig. 4b. It is evident that the response time of both upper and lower steps of the MR damper with a PI control algorithm can be controlled within 16ms. Based on this result, a triangular wave excitation test is conducted following the approach outlined in reference [23], with the test arrangement mirroring that illustrated in Fig. 1. The overall response time is determined based on sampling points during both on and off excitation currents. The global response delay calculation method for an MR damper is represented by (17).

$$\tau = \frac{n_2 - n_1}{f} \times 62.3\% \tag{17}$$

where, n_1 represents the number of points used at the end of the initial state, n_2 denotes the number of sampling points that reached the stable state, and f stands for the sampling frequency. Given the tendency of the electromagnetic response time for up/down steps beyond 1.6A of driving current, this study focuses on measuring the overall response time when the driving current transitions from 0 to 1.6A, resulting in a value of 27.9ms. In other words, it is found that the overall actual response time is lower than the theoretical critical delay allowed by the system to maintain stability.

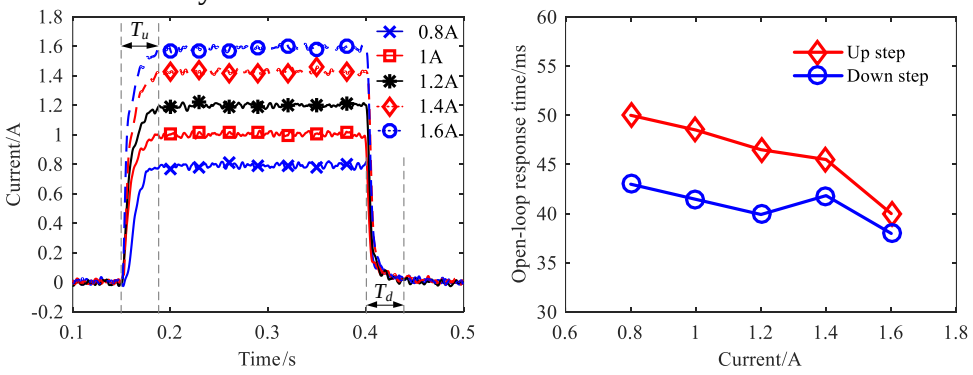

(a) Open-loop control system.

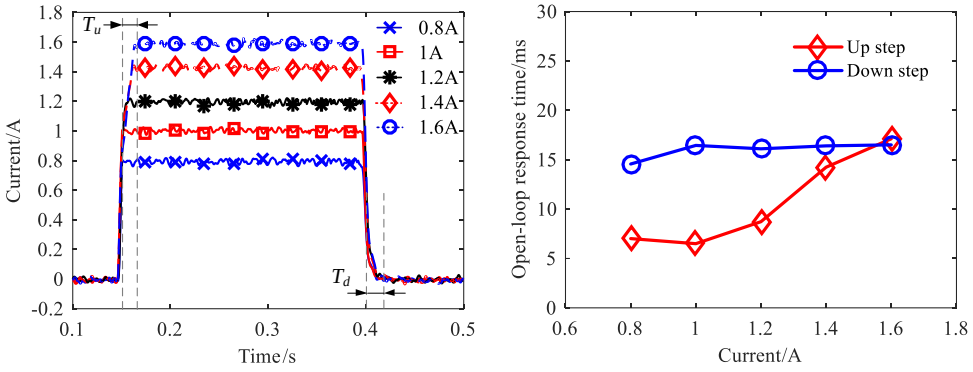

(b) Closed-loop control system.
Fig. 4. Electromagnetic response time.

According to the test results, the feasible solution (feedback gain) of delay dependent H_∞ controller (controller I) is K=10^4×[1.5006 1.6256 -0.1557 -0.0037]. As a comparison, a delay independent H_∞ controller (controller II) is designed, and the controller gain is K=10^4×[2.1345 -0.0122 -0.0011 -0.085].

5. Simulation results

To validate the efficacy of Controller I, a comparison was made between the system dynamic performance under bumpy and random road with that of passive suspension and Controller II. The relevant simulations are conducted. The excitation of the random road can be mathematically found as:

$$\dot{z}_r(t) = -\omega_0 z_r(t) + 2\pi n_0 \sqrt{G_q(n_0)v} \cdot \omega(t), \tag{18}$$

where, $\omega_0 = 2\pi f_0$ denotes the cutoff angle frequency, and $f_0 = 0.01$ represents the cutoff frequency; $\omega(t)$ represents the white noise signal, $z_r(t)$ represents the road profile, v represents the driving speed, $G_q(n_0)$ denotes the road roughness coefficient.

The bump excitation is:

$$z_r = \begin{cases} 0.05 \cdot \left(1 - \cos\dfrac{2\pi v}{L} \cdot t\right), & 0.5\ \text{s} < t < 1\ \text{s} \\ 0, & \text{other} \end{cases}, \tag{19}$$

where v represents the vehicle speed and $v = 10$ m/s denotes selected here, L represents the length of bump and $L = 5$ m is selected.

5.1. Bump road

Figure 5 illustrates the dynamic performance (τ_{act}=27.9ms). Table 1 presents a comparison of the peak to peak responses. It is evident that, in comparison to passive control, controllers I and II exhibit significantly reduced peak to peak responses to each performance index. Specifically, in comparison to passive control, the former reduced by 24.6%, 13.8%, and 7.7%, while the latter decreased by 19.7%, 11.3%, and 15.4% respectively.

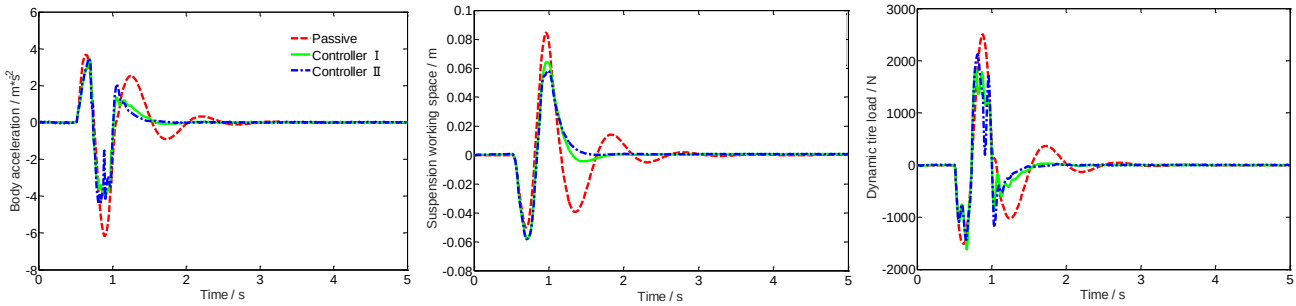

Fig. 5. Dynamic performance comparison.

Tab.1. Peak to peak response comparison.

Index	BA (m/s^2)			SD (m)			DTL (N)		
	Passive	Controller I	Controller II	Passive	Controller I	Controller II	Passive	Controller I	Controller II
Peak-to-Peak	9.85	7.43	7.91	0.13	0.12	0.11	4009	3454	3556
Improvement	-	↓24.6%	↓19.7%	-	↓7.7%	↓15.4%	-	↓13.8%	↓11.3%

5.2. Random road

Figure 6 illustrates the comparison of dynamic performance for each control method under C-grade road conditions ($G_q(n_0)$=256×10^{-6} m^{-1}). Tab.2 presents a comparison of each performance index. It is evident that, in comparison to passive control, the improvement of dynamic performance provided by Controller I and Controller II is primarily manifested in vertical BA and SD, with limited impact on road holding. Specifically, Controller I and Controller II exhibit increases of 19.7% and 13.3% respectively in BA, along with improvements of 30.9% and 16.2% respectively in SD. Furthermore, when compared with Controller II, it can be observed that the BA, SD and DTL are decreased by 7.4%, 17.6%, and 1.1% respectively for Controller I.

The Fourier transform is employed for the analysis of time-domain data in order to obtain the amplitude frequency characteristics of various performance indicators (Fig. 7). It is evident that, in comparison with passive control, Controller I and Controller II have significantly enhanced the low-frequency formant amplitude of each performance index. However, there is no apparent improvement for the high-frequency formant amplitude, indicating that the response delay primarily affects the first-order main mode (*i.e.*, body vibration) of MR SAS, with less impact on the second-order main vibration mode (*i.e.*, wheel vibration) of MR SAS. This finding aligns with the simulation results under bump road excitation.

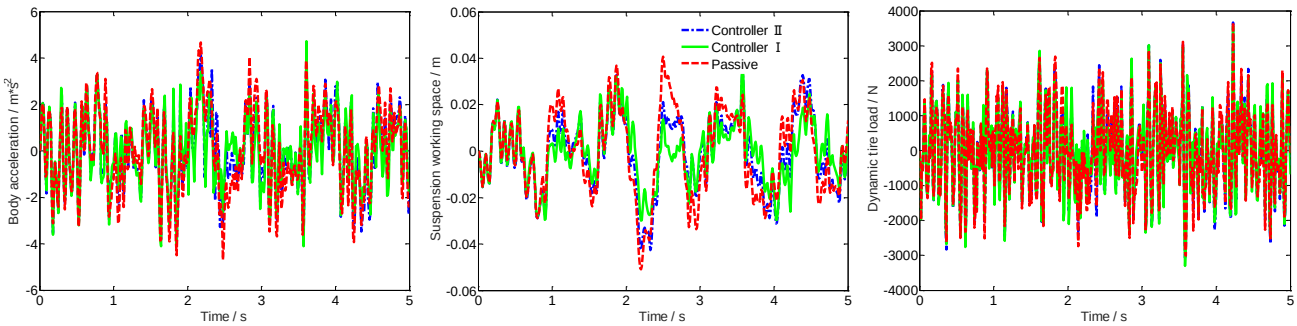

Fig. 6. Dynamic performance comparison.

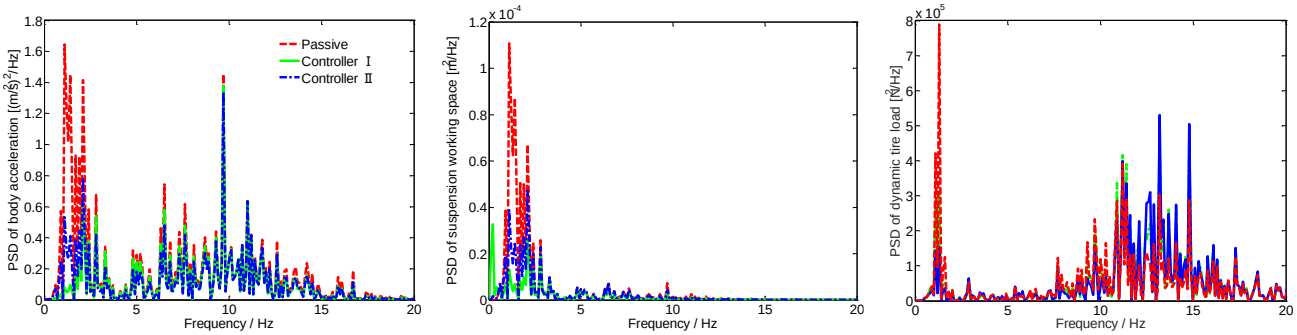

Fig. 7. Amplitude frequency characteristics comparison.

Tab. 2. RMS value comparison of dynamic performances.

Controller	BA (m/s2)	SD (m)	DTL (N)
Passive	1.92	0.021	1166
Controller I	1.54(↓19.7%)	0.014(↓30.9%)	1139(↓2.3%)
Controller II	1.66(↓13.3%)	0.017(↓16.2%)	1151(↓1.3%)

6. Test verification

6.1. Control system design

As shown in Fig. 8a, a quarter McPherson test bench is built for rapid prototyping control test. The test system (Fig. 8b) mainly includes controller, MR damper driver, DC power supply, oscilloscope, acceleration sensor and INSTRON 8800 CNC hydraulic servo vibration test bench.

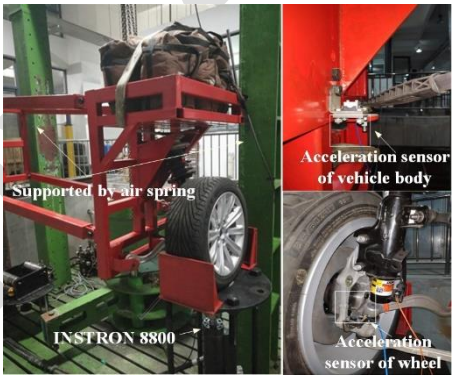

(a) McPherson test bench.

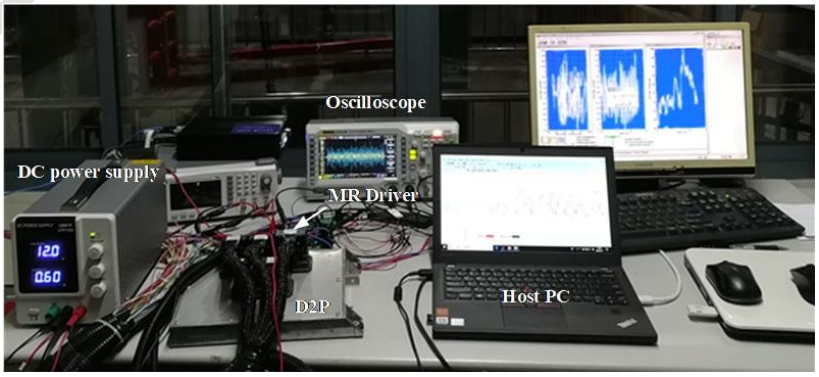

(b) Control system.
Fig. 8. Test bench.

Since the acceleration sensor is only utilized for measuring the vehicle body and wheel acceleration, the state variables required in (9) cannot be directly obtained. Therefore, it is necessary to integrate the acceleration signal once or twice in order to acquire the absolute velocity and displacement respectively. Given that integration often introduces errors into a signal, a combined filter depicted in Fig. 9 has been designed to process the acceleration signal. The combined filter primarily consists of a first-order low-pass filter $L(s)$, $L_i(s)$ for integrating the acceleration signal, and a first-order high-pass filter $H(s)$.

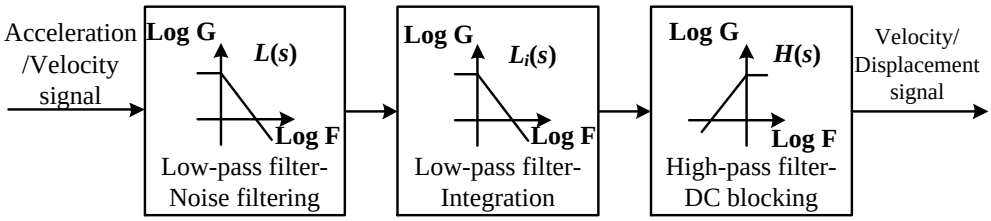

Fig. 9. Combined filter.

Tab. 3 Cut-off frequency.

Filter	$L(s)$	$L_i(s)$	$H(s)$
Cut-off frequency (Hz)	50	0.1	0.5

6.2. Analysis of test results

Figure 9 illustrates the results of dynamic performance testing for each control method under bump road excitation, with the test input being identical to the simulation input. The peak-to-peak response of the three control methods is presented in Tab.4. It is evident that, in comparison to passive control, delay dependent control (Controller I) demonstrates a reduction of 38.6%, 16.7%, and 14.3% in BA, DTL, and SD respectively. Similarly, delay independent control (Controller II) shows a decrease of 26.6%, 25%, and 7.3% compared to passive control for these parameters. Moreover, when comparing delay dependent control (Controller I) with delay independent control (Controller II), it is observed that the peak-to-peak response to vehicle BA and DTL decreases by 16.4% and 7.4% respectively for delay dependent control. Overall, these results indicate significant improvements in reducing peak-to-peak values for BA, DTL, and SD when utilizing both delay dependent and delay independent controls as compared to passive control during bump road excitation testing.

It is important to note that the fluctuation of dynamic performance indexes following bump excitation is attributed to the fact that the single channel test bench is anchored to the ground through an air spring. When the vibration test bench produces pulse excitation, in accordance with the principles of force and reaction force, the entire test bench will vibrate with a specific amplitude. This explains why the acceleration sensor can continue to capture vibration acceleration signals even after the shaking table ceases to output force.

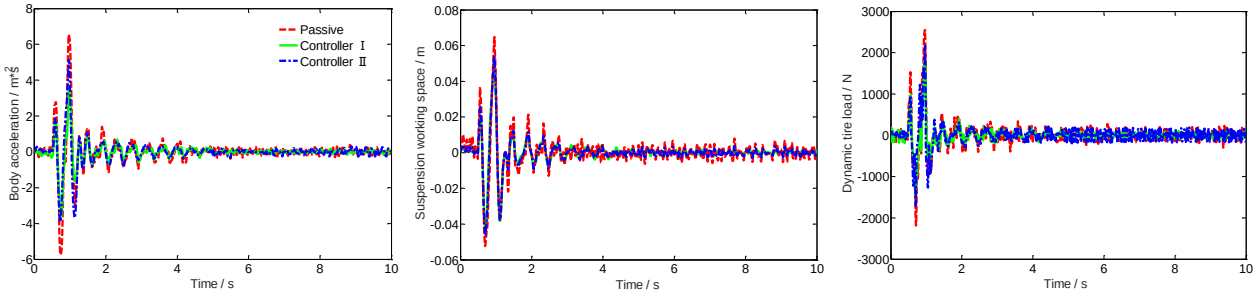

Fig. 10. Dynamic performance test results of different control method under bump road excitation.

Figure 10 depicts the dynamic performance test results of each control method under random road excitation, with the corresponding performance indices provided in Tab.5. It is evident that, when compared to passive control, the enhanced dynamic performance of Controller I and Controller II primarily manifests in reduced vertical BA and SD, while the improvement in road holding is limited, consistent with simulation results. Specifically, in comparison to passive control, both Controller I and Controller II exhibit a decrease of 16.7% and 13.6%, respectively, in BA, as well as reductions of 39.6% and 27.1%, separately, in SD. Moreover, compared to Controller II, a decrease of 3.5% in vertical acceleration, a reduction of 17.l % in SD and an overall decline by 0.89 % of DTL are observed for Controller I. It should be noted that the overall trend of amplitude frequency characteristics for each performance index, aligns with the simulation results. Therefore, further elaboration on this matter will not be provided here.

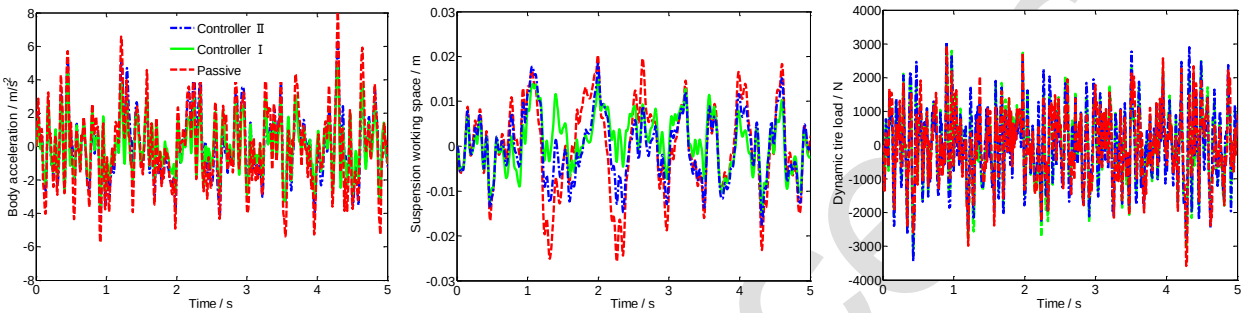

Fig. 11. Dynamic performance test results.

The test results also confirm the efficacy of the proposed control method, with overall trends consistent with the simulation results. However, some discrepancies exist between the simulation and test results, which is shown in Tab. 6 and Tab. 7. Taking Controller I as an example, compared to the simulation results, the BA in the test data is larger, while SD and DTL are decreased. This discrepancy can be attributed to the use of a linear suspension model in the simulation analysis versus a McPherson suspension system with structural nonlinearity in the test verification. In addition to damping force generated by MR damper, friction effects between components also contribute to damping force during testing, resulting in greater actual damping than indicated by simulation analysis. While increased damping is advantageous for reducing SD and DTL, it concurrently leads to higher BA during testing.

Tab. 4. Peak-to-peak response of the three control methods.

Index	BA (m/s^2)			SD (m)			DTL (N)		
	Passive	controller I	controller II	Passive	controller I	controller II	Passive	controller I	controller II
Peak-to-Peak	12.29	7.54	9.02	12.29	7.54	9.02	12.29	7.54	9.02
Improvement	-	↓38.6%	↓26.6%	-	↓38.6%	↓26.6%	-	↓38.6%	↓26.6%

Tab. 5. RMS values of each performance index.

Controller	BA(m/s^2)	SD (m)	DTL (N)
Passive	1.98	0.0096	1156
Controller I	1.65(↓16.7%)	0.0058(↓39.6%)	1110(↓3.97%)
Controller II	1.71(↓13.6%)	0.007(↓27.1%)	1120(↓3.11%)

Tab. 6. Comparison between simulation and test for bump pavement.

	Peak-to-peak value of BA (m/s2)	Peak-to-peak value of SD (m)	Peak-to-peak value of DTL (N)
Simulation	7.43	0.12	3454
Test	7.54	0.1	3306

Tab. 7. Comparison between simulation and test for random road.

	BA (m/s^2)	SD (m)	DTL (N)
Simulation	1.54	0.014	1139
Test	1.65	0.0058	1110

7. Conclusion

This paper presents the design of a time-delay dependent H_∞ robust controller for MR SAS. To address the association between the actual response delay and the theoretical critical delay of the designed delay-dependent controller, a PI control algorithm is developed. The main findings can be summarized as follows:

(1) The simulation results suggest that, in comparison to the delay-independent H_∞ robust controller, the peak-to-peak response of BA and DTL is reduced by 6.1% and 2.9% respectively under bump road conditions, with minimal impact on road holding. When compared to the time delay-independent H_∞ robust control, the vehicle body vertical acceleration, SD, and DTL are reduced by 7.4%, 17.6%, and 1.1% respectively under random road conditions.

(2) The test results indicate that, in comparison with the delay independent H_∞ robust controller, the peak-to-peak response of vehicle BA and DTL is reduced by 16.4% and 7.4% respectively under bump road conditions, with little change in road holding. When compared to the delay independent H_∞ robust control, the BA, SD, and DTL are decreased by 3.5%, 17.1%, and 0.89% respectively under stochastic road conditions.

In the future, further research will be conducted on semi-active suspension control considering system uncertainty, building upon the findings of this paper. Additionally, future research will also take into account the entire vehicle model in order to better align with engineering practice.

Reference

[1] Ding, R., Wang, R., Meng, X., Liu, W., & Chen, L. (2021). Intelligent switching control of hybrid electromagnetic active suspension based on road identification. *Mechanical Systems and Signal Processing*, *152*, 107355. https://doi.org/10.1016/j.ymssp.2020.107355

[2] Sun, X., Wu, M., Yin, C., Wang, S., & Tian, X. (2021). Multiple-Iteration Search Sensorless Control for Linear Motor in Vehicle Regenerative Suspension. *IEEE Transactions on Transportation Electrification*, *7*(3), 1628–1637. https://doi.org/10.1109/tte.2021.3052989

[3] Chen, L., Ding, R., Meng, X., & Wang, R. (2023). Optimal design and experimental research on a new HEMA with energy reduction for vehicle suspension systems. *International Journal of Vehicle Design*, *93*(1/2), 66–86. https://doi.org/10.1504/ijvd.2023.10060273

[4] Liu, W., Wang, R., Ding, R., Meng, X., & Yang, L. (2020). On-line estimation of road profile in semi-active suspension based on unsprung mass acceleration. *Mechanical Systems and Signal Processing*, *135*, 106370. https://doi.org/10.1016/j.ymssp.2019.106370

[5] Cha, Y.-J., Agrawal, A. K., & Dyke, S. J. (2012). Time delay effects on large-scale MR damper based semi-active control strategies. *Smart Materials and Structures*, *22*(1), 015011. https://doi.org/10.1088/0964-1726/22/1/015011

[6] Yoon, D.-S., Park, Y.-J., & Choi, S.-B. (2019). An eddy current effect on the response time of a magnetorheological damper: Analysis and experimental validation. *Mechanical Systems and Signal Processing*, *127*, 136–158. https://doi.org/10.1016/j.ymssp.2019.02.058

[7] Pang, H., Fu, W.-Q., & Liu, K. (2015). Stability analysis and fuzzy smith compensation control for semi-active suspension systems with time delay. *Journal of Intelligent & Fuzzy Systems*, *29*(6), 2513–2525. https://doi.org/10.3233/ifs-151954

[8] Tao, L., Chen, S., Fang, G., & Zu, G. (2019). Smith Predictor-Taylor Series-Based LQG Control for Time Delay Compensation of Vehicle Semiactive Suspension. *Shock and Vibration*, *2019*(1). https://doi.org/10.1155/2019/3476826

[9] Li, G., Gan, Y., Liu, Q., Xu, H., Chen, D., Zhong, L., Deng, J., & Hu, G. (2024). Performance analysis of vehicle magnetorheological semi-active air suspension based on S-QFSMC control. *Frontiers in Materials*, *11*. https://doi.org/10.3389/fmats.2024.1358319

[10] Karim Afshar, K., Javadi, A., & Jahed-Motlagh, M. R. (2018). Robust control of an active suspension system with actuator time delay by predictor feedback. *IET Control Theory & Applications*, *12*(7), 1012–1023. https://doi.org/10.1049/iet-cta.2017.0970

[11] Gu, B., Cong, J., Zhao, J., Chen, H., & Fatemi Golshan, M. (2022). A novel robust finite time control approach for a nonlinear disturbed quarter-vehicle suspension system with time delay actuation. *Automatika*, *63*(4), 627–639. https://doi.org/10.1080/00051144.2022.2059205

[12] Yin, Y., Luo, B., Ren, H., Fang, Q., & Zhang, C. (2022). Robust control design for active suspension system with uncertain dynamics and actuator time delay. *Journal of Mechanical Science and Technology*, *36*(12), 6319–6327. https://doi.org/10.1007/s12206-022-1143-1

[13] Li, J. W., Luo, J. N., Huang, Z. (2024). Study on a semi-active suspension controller considering time delay of CDC system. *Vehicle Engineering*, 46(05), 913-922. https://doi.org/10.19562/j.chinasae.qcgc.2024.05.017

[14] Yang, L. Q., Zhao, Y. Y. (2023). Multi-objective optimization design of a grounded stiffness time delay feedback dynamic vibration absorber with inerter. *Journal of Vibration and Shock*, *42*(23), 133-143.

[15] Liu, C., Chen, L., Zhang, X., & Yang, X. (2020). Stability analysis of semi-active inerter-spring-damper suspensions based on time-delay. *Journal of Theoretical and Applied Mechanics*, *58*(3), 599–610. https://doi.org/10.15632/jtam-pl/121975

[16] Wu, K., Ren, C., & Atay, F. M. (2024). Enhancing energy recovery in automotive suspension systems by utilizing time-delay. *Energy*, *300*, 131578. https://doi.org/10.1016/j.energy.2024.131578

[17] Zhu, M., Lv, G., Zhang, C., Jiang, J., & Wang, H. (2022). Delay-Dependent Sliding Mode Variable Structure Control of Vehicle Magneto-Rheological Semi-Active Suspension. *IEEE Access*, *10*, 51128–51141. https://doi.org/10.1109/access.2022.3173605

[18] Nan, Y., Shao, S., Ren, C., Wu, K., Cheng, Y., & Zhou, P. (2023). Simulation and Experimental Research on Active Suspension System With Time-Delay Feedback Control. *IEEE Access*, *11*, 88498–88510. https://doi.org/10.1109/access.2023.3305265

[19] Hong, S. R., Wereley, N. M., Choi, Y. T., & Choi, S. B. (2008). Analytical and experimental validation of a nondimensional Bingham model for mixed-mode magnetorheological dampers. *Journal of Sound and Vibration*, *312*(3), 399–417. https://doi.org/10.1016/j.jsv.2007.07.087

[20] Ding, R., Wang, R., Meng, X., & Chen, L. (2019). Energy consumption sensitivity analysis and energy-reduction control of hybrid electromagnetic active suspension. *Mechanical Systems and Signal Processing*, *134*, 106301. https://doi.org/10.1016/j.ymssp.2019.106301

[21] El Ghaoui, L., Oustry, F., & AitRami, M. (1997). A cone complementarity linearization algorithm for static output-feedback and related problems. *IEEE Transactions on Automatic Control*, *42*(8), 1171–1176. https://doi.org/10.1109/9.618250

[22] Gouaisbaut, F., & Peaucelle, D. (2006). Delay-dependent stability analysis of linear time delay systems. *IFAC Proceedings Volumes*, *39*(10), 54–59. https://doi.org/10.3182/20060710-3-it-4901.00010

[23] Koo, J.-H., Goncalves, F. D., & Ahmadian, M. (2004). Investigation of the response time of magnetorheological fluid dampers. In K.-W. Wang (Ed.), *SPIE Proceedings* (Vol. 5386, p. 63). SPIE. https://doi.org/10.1117/12.539643